High Current Density Esaki Tunnel Diodes Based on GaSb–InAsSb Heterostructure Nanowires

ARTICLE *in* NANO LETTERS · SEPTEMBER 2011

Impact Factor: 13.59 · DOI: 10.1021/nl202180b · Source: PubMed

NANO LETTERS

LETTER

pubs.acs.org/NanoLett

High Current Density Esaki Tunnel Diodes Based on GaSb-InAsSb Heterostructure Nanowires

Bahram Ganjipour,[†] Anil W. Dey,[‡] B. Mattias Borg,[†] Martin Ek,[§] Mats-Erik Pistol,[†] Kimberly A. Dick,[†,§] Lars-Erik Wernersson,[‡] and Claes Thelander*[,†]

[†]Solid State Physics and [‡]Department of Electrical- and Information Technology, Lund University, Box 118, S-221 00, Lund, Sweden

[§]Polymer and Materials Chemistry, Lund University, Box 124, S-221 00 Lund, Sweden

Supporting Information

ABSTRACT: We present electrical characterization of broken gap GaSb-InAsSb nanowire heterojunctions. Esaki diode characteristics with maximum reverse current of 1750 kA/cm^2 at 0.50 V, maximum peak current of 67 kA/cm^2 at 0.11 V, and peak-to-valley ratio (PVR) of 2.1 are obtained at room temperature. The reverse current density is comparable to that of state-of-the-art tunnel diodes based on heavily doped p-n junctions. However, the GaSb-InAsSb diodes investigated in this work do not rely on heavy doping, which permits studies of transport mechanisms in simple transistor structures processed with high-κ gate dielectrics and top-gates. Such processing results in devices with improved PVR (3.5) and stability of the electrical properties.

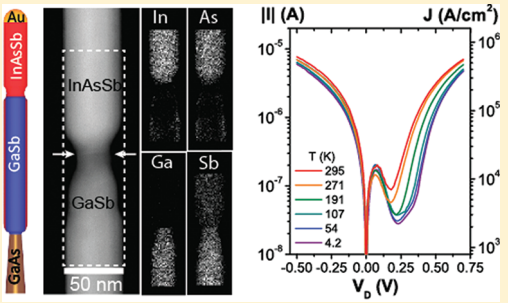

KEYWORDS: Nanowire, Esaki tunnel diode, broken band, heterostructure, InAs, GaSb, tunnel FET

Advances in transistor scaling have led to an increased awareness of the power consumption in digital applications, and methods to reduce both the static and active consumption are studied intensely.[1] Since the main contribution to static power is the subthreshold current, so-called small-swing switches are currently being investigated to complement conventional field-effect transistors (FETs). The importance of such switches is further emphasized by the fact that the active power dissipation shows an almost cubic dependence on operating voltage.[2] For these reasons, tunneling FETs (TFETs), for which sub-60 mV/dec inverse subthreshold slope is possible, have been the subject of numerous investigations for ultra low-power electronic applications.[3−5]

However, to date, experimental results of TFETs have shown poor on-current performance due to a low interband tunneling probability. In this respect, heterostructures of group III/V materials are of interest because of increased heterostructure design potential, narrow bandgaps, and small tunneling masses that allow high efficiency interband tunneling.[6−8] Recent advances in growth of epitaxial semiconductor nanowires (NWs) have allowed studies of new heterojunctions that are of interest to tunneling devices. In particular, the NW technology allows integration of III/V materials with Si, and InAs/Si interband tunnel diodes based on NWs have recently been demonstrated.[9,10] However, among the many possible heterostructure material combinations, InAs-GaSb is potentially the most interesting for tunnel diodes since interband tunneling here occurs without any barrier due to a broken band lineup.[7,11−14] With no requirements of heavy doping or high applied bias- and gate-voltages for interband transport, this junction may become a key element in low-power TFET applications.

In this Letter, we report transport studies of GaSb-InAsSb interband tunneling diodes based on epitaxial NWs. We observe very high tunnel current densities at both forward and reverse bias, comparable to values reported for state-of-the-art tunnel diodes. A negative differential resistance (NDR) region is observed at forward bias, which is explained by an increased band-bending at the interface that eventually disables direct interband tunneling. Finally, conditions for interband tunneling as well as the onset of competing transport mechanisms are studied by investigating the effect of applied top-gate potentials at room temperature and 4.2 K.

GaSb-InAsSb NWs were grown from Au aerosol nanoparticles deposited on GaAs(111)B substrates using metalorganic vapor phase epitaxy. First, a GaAs stem was grown at 470 °C to facilitate nucleation of the GaSb NW.[15] The GaSb segment was grown subsequently using trimethylgallium (TMGa, molar fraction 7.1×10^{-6}) and trimethylantimony (TMSb, 3.4×10^{-5}), followed by an InAs growth step at 460 °C using trimethylindium (TMIn, 4.6×10^{-6}) and arsine (AsH_3, 1.9×10^{-4}). The switching between the GaSb and InAs growth was performed by shutting off the TMGa and TMSb precursors and flowing 2.5 sccm AsH_3 for 10 s, after which InAs growth began by the introduction of TMIn.[16] During growth of the axial InAs segment, a roughly 2−4 nm thick radial InAs shell was also

Received: June 28, 2011
Revised: August 24, 2011
Published: September 06, 2011

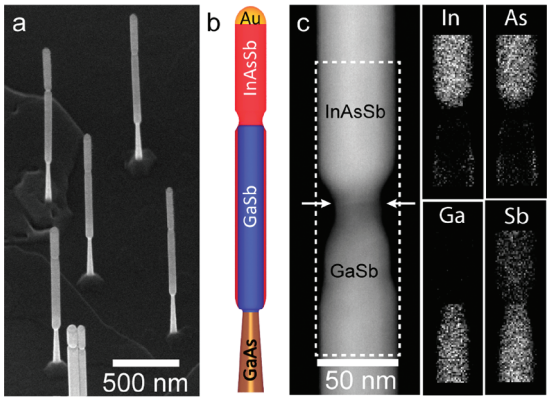

Figure 1. (a) SEM image of GaAs-GaSb-InAsSb heterostructure NWs of Type B (30° tilt). (b) Schematic drawing of the NW chemical composition and morphology. (c) STEM image of the neck region recorded in ⟨112⟩ with insets of Ga Kα, As Kα, In Lα, and Sb Lα XEDS maps (2 × 2 nm pixel size) from the same NW.

formed. The NWs were annealed at 490 °C for 7.5−10 min to locally and selectively etch the InAs shell that surrounds the axial GaSb-InAs heterojunction and to form the neck region seen in Figure 1. As seen in the X-ray energy dispersive spectroscopy (XEDS) mapping in Figure 1c, there is a significant background Sb concentration in the nominal InAs segment, forming a composition of $InAs_{0.9}Sb_{0.1}$. For simplicity, we will refer to this segment, and the shell, as InAsSb.

To investigate the effect of doping on the performance of the tunnel diodes, diethylzinc (DEZn) was introduced during the GaSb growth step. Zn is a p-type dopant in GaSb. We here focus on three different types of NWs, nominally undoped (Type A, DEZn/TMGa = 0), medium Zn precursor flow (Type B, DEZn/TMGa = 0.07) and high Zn precursor flow (Type C, DEZn/TMGa = 0.2). The NWs shown in Figure 1 are of Type B. SEM images of nanowires of Types A and C are shown in Supporting Information.

After growth, NWs were mechanically broken off and transferred to degenerately *n*-doped Si samples capped with 100 nm thick SiO_2. The locations of selected NWs were then determined relative to predefined metal markers using a scanning electron microscope (SEM). Electron beam lithography was used to define Ni/Au contacts to selected NWs, such that two contacts are placed on the GaSb/InAsSb core/shell segments and one contact on the InAsSb axial segment. Prior to contact metal deposition, both the InAsSb and GaSb segments were etched with diluted buffered HF (BHF) for 5 s followed by a rinse in H_2O.

Room-temperature electrical measurements were carried out for individual diodes in darkness and under vacuum conditions, whereas He ambient was used for the low-temperature measurements. In comparison to bare GaSb NWs, processing of low-ohmic contacts to the GaSb segment is here greatly simplified due to the thin InAsSb shell around it. We have found that BHF etching attacks GaSb, but for these devices the InAs shell provides sufficient protection. The strong surface pinning in the conduction band for InAsSb, together with the broken gap at the GaSb-InAsSb heterojunction, seem to allow for very efficient carrier injection. This was verified by first investigating the electrical properties of core/shell GaSb/InAsSb segments. Such segments show low-ohmic and linear $I-V$ for both high positive

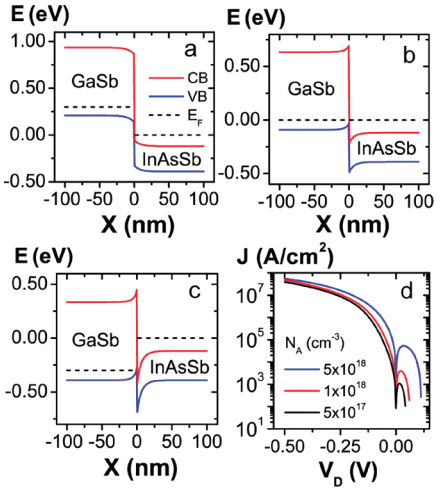

Figure 2. (a−c) Poisson simulation of the band structure for a GaSb-$InAs_{0.9}Sb_{0.1}$ heterojunction with the doping levels set to $p_{GaSb} = 5 \times 10^{17}$ cm^{-3}, $n_{InAsSb} = 1 \times 10^{18}$ cm^{-3} in the case of (a) −0.30 V reverse bias, (b) no bias, (c) 0.30 V forward bias. E_F denotes the quasi Fermi-level. (d) Simulated ideal $J-V$ curves for GaSb/$InAs_{0.9}Sb_{0.1}$ junctions with three different GaSb acceptor doping levels and InAsSb donor level of $N_D = 1 \times 10^{18}$ cm^{-3}.

and negative bias voltages, which means that the voltage drop at the forward-biased GaSb/InAsSb radial junction is not sufficient to suppress tunneling injection. Measurements show an overall weak p-type back-gate dependence suggesting that transport primarily takes place in the core, likely in an accumulation layer at the interface to the InAsSb shell.

Results of Poisson simulations of the bandstructure for the case of an unbiased and biased (V_D = −0.30 V, +0.30 V) axial GaSb-$InAs_{0.9}Sb_{0.1}$ heterojunction are shown in Figure 2a−c. The fixed band-offset between the GaSb valence band and the InAsSb conduction band is here set to −190 mV at the heterojunction.[17] The Poisson simulation in Figure 2c indicates that a mechanism of NDR should occur, which is related to an increased band bending at forward bias, where a strong confinement on either side of the heterojunction develops with increasing positive V_D. Eventually the lowest conduction sub-band on the InAs side is pushed above the highest light hole sub-band on the GaSb side, which disables direct band-to-band tunneling. Such NDR was observed by Collins et al.[11] for GaSb-InAs planar tunnel diodes although no mechanism was proposed.

We have performed numerical calculations of the tunneling currents across the GaSb-InAsSb heterojunction in the ideal case of no scattering and omitting effects of a 1D (radial) confinement from the nanowire structure. Kane's two-band k·p model[18] was used for the calculation of the energy dispersion and density of states of conduction band electrons and light holes. For a given bias the band structure potential was obtained from the Poisson equation and the corresponding tunnel current was calculated within the Landauer-Büttiker formalism.[19] The transmission coefficients through the depletion tunnel barriers in reverse bias were estimated from the Wentzel−Kramers−Brillouin (WKB) approximation. For the broken gap energies, a transmission coefficient value of 0.4 was used, consistent with ref 11. The WKB approximation was also used to estimate the lowest sub-band energies in the notch regions by assuming Bohr−Sommerfeld quantization. The resulting $J-V$ curves for three

dx.doi.org/10.1021/nl202180b |*Nano Lett.* 2011, 11, 4222–4226

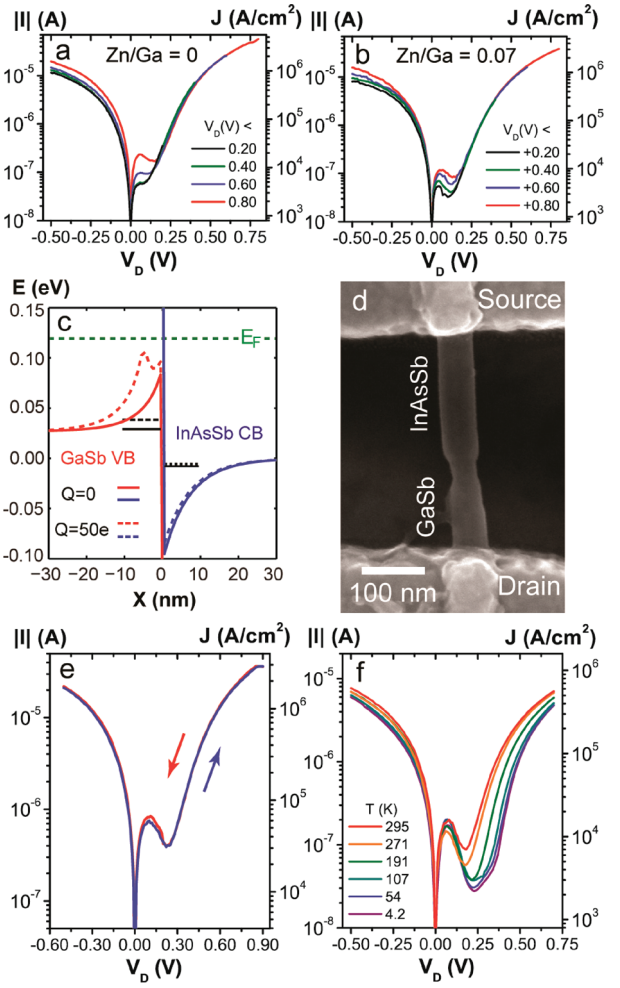

Figure 3. (a) $|I|-V_D$ sweeps at room temperature for different V_D sweep magnitudes for a NW of Type A. (b) The same measurement as in panel a, but for a NW of Type B. (c) Simulation of the GaSb-InAsSb interface with and without an extra negative 50e charge inserted 5 nm from the interface on the GaSb side. The black lines indicate the energy of the lowest sub-band in the wells. The extra charge broadens the GaSb well (dashed) and lifts up the light-hole sub-band. (d) Top-view SEM of an electrically contacted GaSb-InAsSb heterojunction NW of Type B with a short source−drain distance. (e) Forward (blue) and reverse (red) $|I|-V_D$ sweeps for the NW in panel d (Type B) showing the highest reverse current density and forward peak current density. (f) $|I|-V_D$ sweep for temperatures in the range 4.2 to 295 K, where the reverse and peak currents are affected only marginally, whereas the excess forward current is substantially reduced at lower T.

different GaSb doping levels are shown in Figure 2d. The simulation shows that doping should have a substantial effect on the current density for low bias, whereas the relative effect of the doping is much weaker at high negative bias, assuming effects of series resistance outside of the junction region are neglected. Higher doping also allows forward interband tunneling at higher positive V_D, thereby considerably increasing the forward peak current density.

In the electrical studies of axial heterojunction GaSb-InAsSb devices, the end of the InAsSb segments was grounded and the drain voltage, V_D, was applied to the GaSb end. Room temperature $I-V$ characteristics of a nominally intrinsic (Type A) GaSb-InAsSb tunnel diode with a neck diameter of 40 nm are shown in Figure 3a. For positive V_D, a nonlinear $I-V$ is observed, where the nonlinearity becomes progressively stronger with increasing voltage sweep magnitude. For a V_D sweep magnitude of 0.50 V a NDR region is visible, which is a typical signature of interband tunneling. The strongly bias-dependent behavior indicates charging of states close to the heterojunction where it seems to affect the local band bending. This is also manifested as a small positive shift of the peak position with increasing V_D, as well as an increase in the reverse tunnel current. We believe that the charging mechanism, which seems to have a decay time on the order of minutes (Supporting Information), is an effect of surface states rather than deep levels, for which decay times on the order of ns are expected.[20] Other possible sources may be defects associated with the presence of hydrogen in the GaSb, or DX-like centers with very high activation energy.[21,22] In Figure 3c, the band-structure for a case of trapped negative charges 5 nm from the junction in the GaSb has been simulated. The distance was chosen arbitrarily; however the simulation shows qualitatively that such charges can strongly affect the band-bending and lead to a larger effective overlap between the conduction and valence sub-bands.

Figure 3b shows $I-V$ characteristics for a NW of Type B (medium DEZn flow). Also in this case an effect of V_D sweep magnitude was observed for the reverse- and forward peak tunnel-currents. However, as the figure indicates, these NWs typically showed NDR even with no history of high forward bias. Furthermore we note that the peak-to-valley ratio is almost constant for the different sweep magnitudes. No systematic increase in reverse bias tunnel current ($V_D = -0.5$ V) could be observed for samples where DEZn was used. This is in qualitative agreement with the results of the simulation in Figure 2d if we only consider the junction itself and disregard series-resistance. We therefore speculate that the Zn doping primarily is manifested in the measurements as an increase in the effective conduction-valence band overlap at forward bias, thus contributing to a visibly higher band-to-band tunneling current only in this bias direction.

Figure 3e shows $I-V$ characteristics (forward and reverse sweep) at room temperature for a NW of Type B with a very short (100 nm) GaSb drain segment length (Figure 3d). This NW had the highest observed reverse- and forward-tunnel current densities. For $V_D = -0.50$ V a reverse current of $I_{rev} = 22\ \mu$A is observed. This corresponds to a scaled current density of $J_{rev} = 1750$ kA/cm^2, where a cross-sectional diameter of $D = 40$ nm has been used for the constriction. Corresponding values for the peak at forward bias ($V_D = 0.11$ V) is $I_{peak} = 840$ nA, $J_{peak} = 67$ kA/cm^2, with a minimum valley current ($V_D = 0.22$ V) of $I_{valley} = 400$ nA, giving a peak-to-valley ratio of 2.1.

The reverse current density of 1750 kA/cm^2 is considerably higher than other reported nanowire III−V tunnel junctions[23] and Si-InAs heterojunctions[10] and is comparable to the highest overall reported number by Mohata et al. for MBE grown $In_{0.53}Ga_{0.47}As$ Esaki diodes of just below 2000 kA/cm^2 at a bias of −0.50 V.[8]

The reverse current starts to show a linear increase for $V_D < -0.15$ V. This may be related to the fixed valence-conduction-band offset of −0.19 V at the heterojunction that sets a limit to the reverse band-to-band tunneling. Simulations show that flat-band condition should be reached at around −0.15 V, after which a depletion-type band bending sets in (Figure 2a). However, it may also be an indication that series resistances are dominating the transport. For core/shell sections of the GaSb-InAsSb NWs

dx.doi.org/10.1021/nl202180b |Nano Lett. 2011, 11, 4222–4226

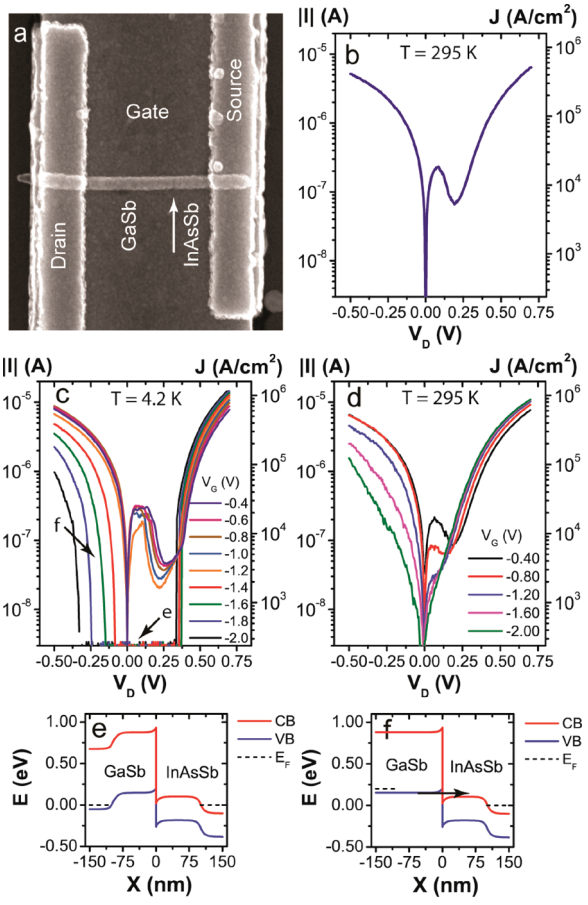

Figure 4. (a) SEM image of a GaSb-InAsSb tunnel diode of Type B processed with 10 nm HfO_2, and Ni/Au top-gate that also covers the source and drain electrodes (b) NW of Type B processed identically to the NW in panel a with the best room-temperature PVR = 3.5. (c) $|I|-V_D$ curves at $T = 4.2$ K in a top-gate voltage range $-0.4\ \text{V} < V_G < -2.0\ \text{V}$ for the NW in panel a (Type B) processed with HfO_2 dielectric and a metal top-gate. (d) The same device as in panel c measured at $T = 295$ K. (e) Schematic drawing of the band diagram for the case of a negative applied top-gate potential that blocks transport as indicated with an arrow in panel c. (f) Same as in panel e, but with a sufficiently large negative drain voltage applied to the GaSb to overcome the gate-induced barrier, also indicated with an arrow in panel c.

of Type B, we find a resistivity in the range of 20−30 mΩcm, which is typically a factor of 10 higher than for the InAsSb sections. This implies that the GaSb segment is the primary source of series resistance. For the 100 nm GaSb segment in Figure 3d, we estimate a resistance of at least 10−15 kΩ, which is almost half of the total diode resistance. A simulated ideal $I-V$ curve (c.f. Figure 2d) yields an excellent fit in reverse bias to the data in Figure 3e using a series resistance of 10 kΩ and $N_A(\text{GaSb}) = 2 \times 10^{18}\ \text{cm}^{-3}$, $N_D(\text{InAsSb}) = 1 \times 10^{18}\ \text{cm}^{-3}$. We therefore expect to be able to further increase the current densities in these structures by reducing the device length, and by increasing the carrier concentrations in the GaSb/InAsSb core/shell segment through doping.

Figure 3f shows the observed temperature-dependent $I-V$ of a device of Type B, where the PVR of 2.2 at room temperature increases to 6.6 at 4.2 K. The weak but finite temperature dependence of the reverse current density can partly be explained by a small change in band gap and band offset with temperature but also by an increased series resistance of the GaSb segment at lower temperatures.

Diodes with the highest studied Zn-precursor flow, Type C, had even higher reverse current densities, but the devices did not show NDR at room temperature. Here we cannot rule out the possible contribution from an incompletely etched thin InAs shell at the heterojunction providing an alternate current path, although we speculate that the lack of NDR is an effect of increased tunneling via impurity states in the band gap. Regions with NDR typically appeared at temperatures below 200 K also for these devices (Supporting Information).

Finally, top-gates were fabricated onto the heterojunction NWs of Type B in order to study the effect of an applied electrostatic gate potential on the transport. The top-gates fully covered both the GaSb and InAsSb segments in between the prefabricated source- and drain-electrodes. A 10 nm thick layer of HfO_2 was deposited using atomic layer deposition (Picosun SUNALE R-100) at 100 °C using a lift-off technique[24] followed by another EBL pattering step and Ni and Au evaporation (Figure 4a). Figure 4b shows an $I-V$ sweep at room temperature for a device with the best PVR = 3.5 for $V_G = 0$ V. This result shows that the high-κ process does not increase the excess current in the valley region. Interestingly this device, and many other devices processed identically, did not show a memory effect for increasing forward bias range, which strengthens the hypothesis that the origin of the defects is related to the NW surface. However, some NWs with identical processing conditions still showed a memory effect, pointing to device-to-device variations.

Figure 4c shows $I-V$ sweeps for applied top-gate voltages (V_G) in the range −0.4 to −2.0 V at $T = 4.2$ K for the NW shown in Figure 4a. For $V_G > -1.3$ V, the InAsSb conduction band edge is below the Fermi level, allowing direct interband tunneling, with a maximum peak-to-valley ratio close to 10 in the forward direction. For $V_G < -1.3$ V the InAsSb segment becomes fully depleted of electrons, which leads to an abrupt blockade of direct interband tunneling and that no peak is observed in forward bias. This situation is depicted schematically in Figure 4e. By applying a negative V_D the gate-induced barrier in the InAsSb segment can be overcome such that reverse bias tunneling is possible, depicted in Figure 4f. For V_D around 0.35 V a very abrupt increase in the current is observed (the bandgap of $InAs_{0.9}Sb_{0.1}$ is 0.34 eV at $T = 4.2$ K). We interpret this as the onset of hole-tunneling in the valence band from GaSb to InAsSb. As expected, the current here shows a reverse gate-dependence compared to electron transport.

Figure 4d shows the $I-V$ of the same device at room temperature. At this temperature the effect of an applied gate potential is less pronounced since the InAsSb segment cannot be fully depleted in the studied V_G range, and only a suppression of the low-bias current for negative V_G is observed. This may be related to hole transport due to the relatively large negative V_D applied. Otherwise the device shows the same overall behavior, where a peak is observed in the forward bias direction for $V_G > -1$ V at the onset of forward interband tunneling.

In conclusion, the electrical properties of heterostructure interband tunnel junctions in GaSb-InAsSb nanowires have been studied. We find reverse tunnel current densities comparable to the highest reported to date for other technologies. Modeling shows that the current densities in these structures can be increased further by minimizing parasitic series resistances. Furthermore, we find that the electrical properties may be

dx.doi.org/10.1021/nl202180b |*Nano Lett.* 2011, 11, 4222–4226

affected by charges trapped near the junction, shifting the energy line-up between the valence and conduction states to which the device operation is very sensitive. Diodes processed with high-κ dielectrics and top-gate electrodes showed PVR up to 3.5 at room temperature as well as more stable electrical properties, which is promising for future TFET studies based on these structures.

■ ASSOCIATED CONTENT

Supporting Information. Additional figures. This material is available free of charge via the Internet at http://pubs.acs.org.

■ AUTHOR INFORMATION

Corresponding Author
*E-mail: Claes.Thelander@ftf.lth.se.

■ ACKNOWLEDGMENT

This work was carried out with financial support from the Nanometer Structure Consortium at Lund University (nmC@LU), the Swedish Research Council (VR), the Swedish Foundation for Strategic Research (SSF), and the Knut and Alice Wallenberg Foundation (KAW).

■ REFERENCES

(1) Nilsson, P. IEEE 13th International Conference on Electronic, Circuits and Systems, December 10-13, 2006, 656−659; IEEE: Nice, France.
(2) Chang, L.; Frank, D. J.; Montoye, R. K.; Koester, S. J.; Ji, L. B.; Coteus, P. W.; Dennard, R. H.; Haensch, W. *Proc. IEEE* . **2010**, *98*, 215.
(3) Zhao, H.; Chen, Y.; Wang, Y.; Zhou, F.; Xue, F.; Lee, J. *IEEE Electron Device Lett.* **2010**, *31*, 1392.
(4) Choi, W. Y.; Park, B. -G.; Lee, J. D.; King Liu, T.-J. *IEEE Electron Device Lett.* **2007**, *28*, 743.
(5) Appenzeller, J.; Lin, Y.-M.; Knoch, J.; Avouris, Ph. *Phys. Rev. Lett.* **2004**, *93*, 196805.
(6) Verhulst, A. S.; Vandenberghe, W. G.; Maex, K.; De Gendt, S.; Heyns, M. M.; Groeseneken, G. *IEEE Electron Device Lett.* **2008**, *29*, 1398.
(7) Knoch, J.; Appenzeller, J. *IEEE Electron Device Lett.* **2010**, *31*, 305.
(8) Mohata, D. K.; Pawlik, D.; Liu, L.; Mookerjea, S.; Saripalli, V.; Rommel, S.; Datta, S. Device Research Conference, June 21-23, 2010, 103−104; IEEE: South Bend, Indiana.
(9) Tomioka, K.; Fukui, T. *Appl. Phys. Lett.* **2011**, *98*, 083114.
(10) Björk, M. T.; Schmid, H.; Bessire, C. D.; Moselund, K. E.; Ghoneim, H.; Karg, S.; Lörtscher, E.; Riel, H. *Appl. Phys. Lett.* **2010**, *97*, 163501.
(11) Collins, D. A.; Yu, E. T.; Rajakarunanayake, Y.; Soderstrom, J. R.; Ting, D. Z.-Y.; Chow, D. H.; McGil, T. C. *Appl. Phys. Lett.* **1990**, *57*, 683.
(12) Borg, B. M.; Dick, K. A.; Ganjipour, B.; Pistol, M. E.; Wernersson, L.-E.; Thelander, C. *Nano Lett.* **2010**, *10*, 4080.
(13) Sakaki, H.; Chang, L. L.; Ludeke, R.; Chang, Chin-An.; Sai-Halasz, G. A.; Esaki, L. *Appl. Phys. Lett.* **1977**, *31*, 211.
(14) Koswatta, S. O.; Koester, S. J.; Haensch, W. Proceedings of the 2009 International Electron Devices Meeting (IEDM), December 14-16, 2009, 1−4; IEEE: Baltimore, Maryland.
(15) Jeppsson, M.; Dick, K. A.; Wagner, J. B.; Caroff, P.; Deppert, K.; Samuelson, L.; Wernersson, L.-E. *J. Cryst. Growth* **2008**, *310*, 4115.
(16) Ek, M.; Borg, B. M.; Dey, A. W.; Ganjipour, B.; Thelander, C.; Wernersson, L.-E.; Dick, K. A. Accepted *Cryst. Growth Des.,* DOI: 10.1021/cg200829q.
(17) Vurgaftman, I.; Meyer, J. R.; Ram-Mohan, L. R. *J. Appl. Phys.* **2001**, *89*, 5815.
(18) Kane, E. O. *J. Phys. Chem. Solids* **1957**, *1*, 249.
(19) Büttiker, M. *Phys. Rev. B* **1988**, *38*, 9375.
(20) Lanza, C. *Solid-State Electron.* **1964**, *7*, 733.
(21) Dutta, P. S; Sangunni, K. S.; Bhat, H. L.; Kumar, V. *Appl. Phys. Lett.* **1995**, *66*, 1986.
(22) Hubik, P.; Smid, V.; Kristofik, J.; Stepanek, B.; Sestakova, V. *Solid State Commun.* **1993**, *86*, 19.
(23) Wallentin, J.; Persson, J. M.; Wagner, J. B.; Samuelson, L.; Deppert, K.; Borgström, M. T. *Nano Lett.* **2010**, *10*, 974.
(24) Biercuk, M. J.; Monsma, D. J.; Marcus, C. M.; Becker, J. S.; Gordon, R. G. *Appl. Phys. Lett.* **2003**, *83*, 2405.